Rotation of Edge Localized Modes and their Filaments

J.A. Morales[1], M. Bécoulet[1], F. Orain[1], X. Garbet[1], G. Dif-Pradalier[1],
C. Passeron[1] and G.T.A. Huijsmans[2]

[1] *CEA / IRFM, Cadarache, 13108, St-Paul-Lez-Durance, France*

[2] *ITER Organization,† Route de Vinon-sur-Verdon, CS 90 046, 13067, St-Paul-Lez-Durance, France*

Important to the edge localized modes (ELM) dynamics, the rotation of the ELM and their associated filaments has recently been measured during the ELM crash in KSTAR [1] and in ASDEX Upgrade [2]. It is unclear which mechanism is responsible for the ELM rotation, either the $\boldsymbol{E}\times\boldsymbol{B}$ or the diamagnetic velocity during the growth phase of the ELM.

To study this problem we have carried out analytical linear calculations and numerical simulations of the ELM rotation using the reduced magnetohydrodynamic JOREK code [3]. Plasma flows such as the toroidal rotation, the bi-fluid diamagnetic effects, and neoclassical poloidal friction were recently implemented in the code [4]. The introduction of flows in the numerical model demonstrated the emergence of a strong ELM rotation due to the presence of the diamagnetic effects. We show here that the combination of the diamagnetic, $\boldsymbol{E}\times\boldsymbol{B}$ and parallel velocities is responsible for the ELM rotation in the growth phase. A simple relation is found based on theoretical considerations.

Analytical analysis of the ballooning instability rotation

To calculate the dispersion relation associated to the ballooning instability the reduced MHD equations are considered. We use the gyro-viscous cancellation to simplify the equation over the electric potential (see e.g. [5]). The ballooning representation is used to reduce the two-dimensional problem to one dimension (see e.g. [6]). The following ansatz is considered

$$\tilde{\Phi}(r,\theta,\varphi,t) \approx \widehat{\Phi}(\theta) e^{i[n(\varphi-q\theta)-\omega t]}, \tag{1}$$

for simplification we consider that we are placed in the plasma rotating reference frame, hence $\widehat{\Phi}_0 = 0$.

Using these hypothesis the following dispersion relation is found

$$\omega(\omega-\omega_i^*)\left[(\omega-\omega_e^*)+\frac{q^2R_0^2\left(\omega-\omega_e^*+i\eta k_\theta^2\right)^2}{i\eta k_\theta^2 s^2}\left[\omega\left(\omega-\omega_i^*\right)+2\gamma_I^2\right]\right] \quad + \\ \gamma_I^2(\omega-\omega_e^*)\left(1+\frac{\left(\omega-\omega_e^*+i\eta k_\theta^2\right)\left(2s(1-s)-1\right)}{2i\eta k_\theta^2 s^2}\right) = \frac{-q^2R_0^2\left(\omega-\omega_e^*+i\eta k_\theta^2\right)^2}{i\eta k_\theta^2 s^2}\gamma_I^4, \tag{2}$$

†The views and opinions expressed herein do not necessarily reflect those of the ITER Organization.

$$\text{with} \quad \omega_i^* = -\omega_e^* = \tau_{IC}\frac{\partial P_0}{\partial r} k_\theta \, \boldsymbol{e}_\theta, \qquad \tau_{IC} = \frac{1}{\omega_{Ci}\tau_A} = \frac{m_i}{eR_0\sqrt{\rho_0\mu_0}} \qquad \text{and} \qquad \gamma_I = \left\{ -\frac{4}{B_0 R_0}\frac{\partial P_0}{\partial r} \right\}^{1/2}. \quad (3)$$

The parameter τ_{IC} is the diamagnetic parameter and γ_I the ideal interchange mode growth rate. For the notations see Ref. [4].

At the resistive ($\eta \to \infty$) and strong magnetic shear ($s >> 1$) limit this expression simplifies to

$$\omega(\omega - \omega_i^*)(\omega - \omega_e^*) = \left(i\gamma_\eta\right)^3 \qquad \text{with} \qquad \gamma_\eta = \left[\frac{k_\theta^2 q^2}{s^2} R_0^2 \eta \gamma_I^4 \right]^{1/3}. \quad (4)$$

Considering $\omega_i^* = -\omega_e^* = \omega_*$, the roots of the polynomial can be found using Cardano's method. We also consider the change of variable, $\omega = i\gamma$, the dispersion relation can be simplified to

$$\gamma\left(\gamma^2 + \omega_*^2\right) = \gamma_\eta^3. \quad (5)$$

Two limits can be identified in Eq. (5) for $\gamma_\eta >> \omega_*$ the solution $\gamma \approx \gamma_\eta$ and if $\gamma_\eta << \omega_* \longrightarrow \gamma \approx \gamma_\eta^3/\omega_*^2$. In the general case three roots exist, one real and two complex conjugates, as also found in [7]. The most unstable root is always the real one, as $\omega = i\gamma$, the value of ω is pure imaginary, hence at this limit the unstable mode does not rotate.

Also we can consider the ideal case, $\eta \to 0$, and small magnetic shear ($s \approx 1$). In this case the dispersion relation Eq. (2) simplifies to the second order polynomial

$$\omega^2 - \omega_i^*\omega + \gamma_I^2 = 0. \quad (6)$$

Two distinct roots exist

$$\omega_{1,2} = \frac{\omega_i^* \pm \sqrt{\omega_i^{*2} - 4\gamma_I^2}}{2}. \quad (7)$$

The system is ideally unstable if: $\omega_i^{*2} < 4\gamma_I^2$. And the ideal rotation frequency of the mode is: $\omega_i^*/2$, as also explained in [8]. In this case the unstable mode rotates at half of the diamagnetic frequency in the ion diamagnetic direction.

The roots of the general dispersion relation, Eq (2), are computed numerically. We find that in realistic cases, i.e., at low resistivity ($\eta < 10^{-7}$) the most unstable root is close to the solution at the zero resistivity small shear limit, Eq. (7). In Fig. 1 three computed cases are compared to the analytical solution Eq. (7). One can observe that the imaginary part of the root is

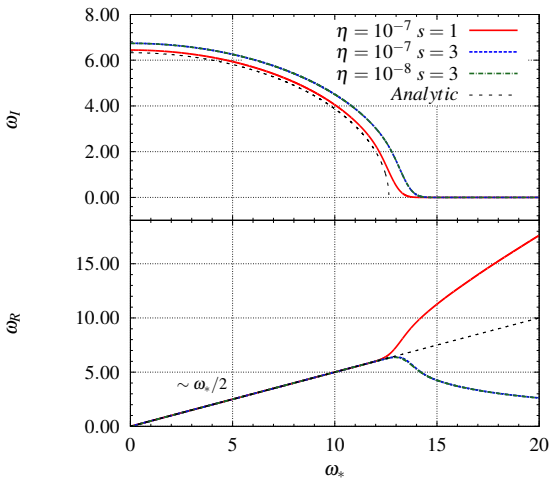

Figure 1: *Evolution of the roots with with the diamagnetic frequency* ω_*.

close to the theory if the shear is small. With increasing shear, the mode is more unstable. On the other hand the real part of the root matches very well the analytical solution. The rotation of the mode in the rotating plasma reference frame is $\omega_*/2$, this was also found in [8].

From this analysis we expect to find the ELM in the JOREK numerical simulations rotating with the plasma plus half the diamagnetic velocity V^*. The mode speed in the poloidal plane (along the flux surfaces) can be written

$$V_{mode} = V_{\boldsymbol{E}\times\boldsymbol{B}} + V_{/\!/} \cdot b_\theta + \frac{V^*}{2}. \tag{8}$$

Numerical simulations and comparison with the theory

The JOREK simulations are performed with two toroidal modes $n = 0$ and $n = 6$. For the considered geometry and initial condition the plasma is unstable for the $n = 6$ toroidal mode. The energy of this mode grows and saturates (see Fig. 2 (left)). The growth rate of the mode decreases if the diamagnetic parameter τ_{IC} is increased. In Fig. 2 (right) we observe that the mode rotates faster if the diamagnetic effects are included. For all the simulations we find that the rotation is in the electron diamagnetic or $\boldsymbol{E}\times\boldsymbol{B}$ direction. It is important to note that the rotation of the modes is quasi-uniform. In Fig. 3 (left) the radial profiles of the mode rotation speed do not show a strong shear. These profiles are calculated following the displacement of the maxima of the modes during the linear growth phase along the flux surfaces in the poloidal plane.

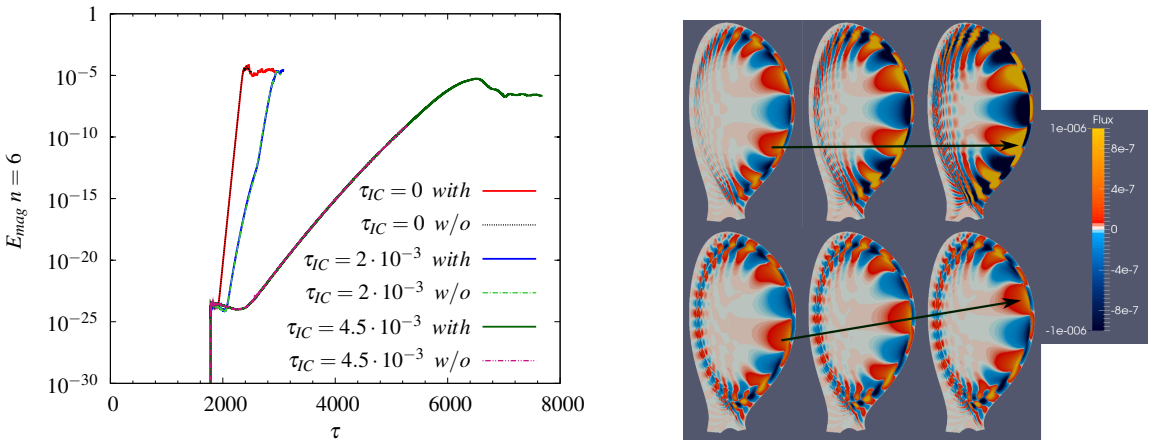

Figure 2: ***(Left)*** *Magnetic energy of the toroidal $n = 6$ mode for 3 values of the diamagnetic parameter τ_{IC} with neoclassical tensor and parallel velocity source, noted with the keyword with, and without this two features, noted as w/o. For all cases $\eta = 10^{-7}$.* ***(Right)*** *Magnetic flux perturbations, with a toroidal mode number $n = 6$, for three different times, with fixed 20 Alfvén times between each image. Without diamagnetic effects (top) and with diamagnetic effects (bottom). The rotation is anticlockwise, i.e. in the electron diamagnetic or $\boldsymbol{E}\times\boldsymbol{B}$ direction.*

In Fig. 3 (right) we show the velocity profile of the mode V_{mode} calculated with the analytical Eq. (8). We observe that even if the diamagnetic velocity V^* is in the ion diamagnetic direction (by convention here negative) the plasma motion ($V_{\boldsymbol{E}\times\boldsymbol{B}}$ plus $V_{/\!/} \cdot b_\theta$) compensates and makes the modes rotate in the opposite direction (positive). In fact at the position of the strong pressure gradient (pedestal) the total velocity of the mode V_{mode} is always in the electron diamagnetic or $\boldsymbol{E}\times\boldsymbol{B}$ direction.

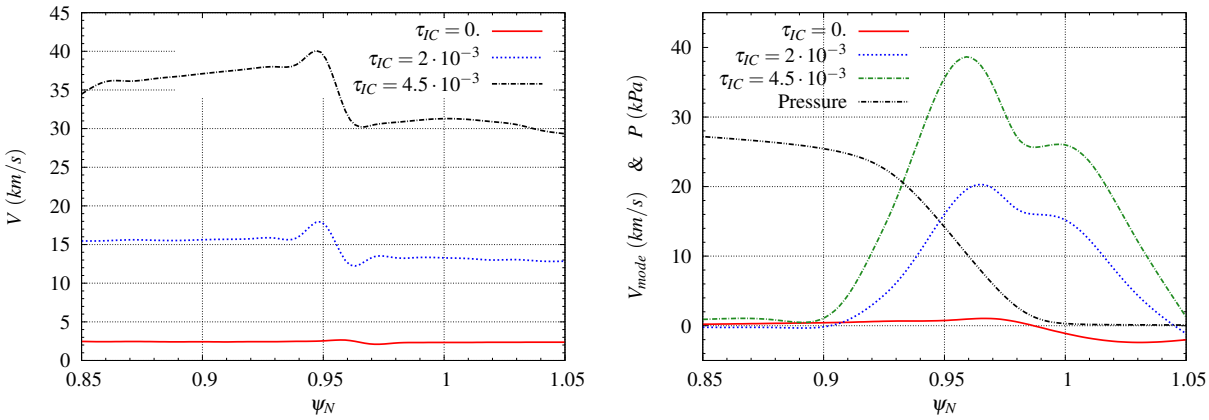

Figure 3: *The positive velocity convention means in the electron diamagnetic or* $\boldsymbol{E}\times\boldsymbol{B}$ *direction.* ***(Left)*** *Radial profile of the ELM rotation velocity along the flux surfaces.* ***(Right)*** *Radial profile of the poloidal velocity* V_{mode} *defined in Eq.* (8) *and pressure profile.*

To quantify the rotation velocity of the ELM in the linear phase we plot, Fig. 4, the velocity of the modes inside the separatrix (extracted from the profiles Fig. 3 (left) for $\psi_N < 0.95$) as a function of the diamagnetic parameter (defined in Eq. (3)). This is done for different resistivities and parallel thermal diffusivities ($\kappa_{/\!/}$). We observe in Fig. 4 that the rotation does not depend greatly on the resistivity and parallel conductivity. The rotation velocity evolves linearly with the diamagnetic parameter τ_{IC} in agreement with Eq. (8). In fact V_{mode} scales as $\approx V_{\boldsymbol{E}\times\boldsymbol{B}} + V^*/2$. We can do the approximation that $V_{\boldsymbol{E}\times\boldsymbol{B}}$ is proportional to τ_{IC} at the pedestal (in this region the electron pressure gradient is the most important component of the radial electric field). If the $\boldsymbol{E}\times\boldsymbol{B}$ velocity is defined in the positive direction the ELM velocity scales approximately as

$$V_{mode} \approx V_{\boldsymbol{E}\times\boldsymbol{B}} + \frac{V^*}{2} \quad \propto \quad \tau_{IC} - \frac{\tau_{IC}}{2} = +\frac{\tau_{IC}}{2}, \tag{9}$$

in the electron diamagnetic or $\boldsymbol{E}\times\boldsymbol{B}$ velocity direction. This velocity direction and the magnitude of the speed of the ELM rotation (several km/s) are in agreement with the experimental observations (e.g. [1, 2]).

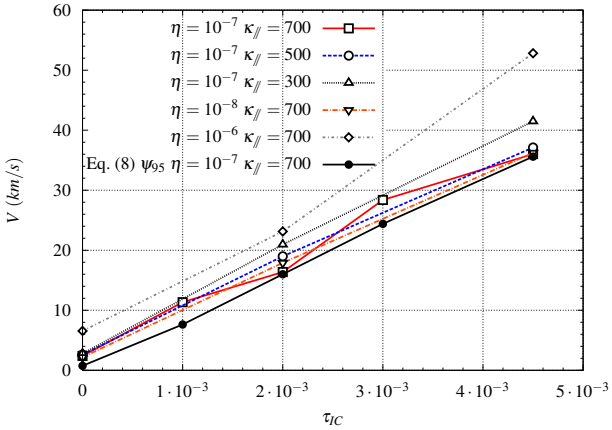

Figure 4: *Rotation velocity of the ELM as a function of the diamagnetic parameter and comparison with the analytical expression Eq.* (8) *taked at* ψ_{95} *(i.e. at the pedestal).*

References

[1] G.S. Yun *et al.*, Phys. Rev. Lett. **107**,4 (2011)

[2] I.G.J. Classen *et al.*, Nuclear Fusion **53**,7 (2013)

[3] G.T.A. Huysmans *et al.*, Plasma Phys. Control. Fusion **51**,12 (2009)

[4] F. Orain *et al.*, Phys. of Plasmas **20**,10 (2013)

[5] D.D Schnack *et al.*, Phys. of Plasmas **13**,5 (2005)

[6] J.W. Connor *et al.*, Phys. Rev. Lett. **44** (1978)

[7] P.H. Diamond *et al.*, Phys. of Fluids **28**,4 (1985)

[8] G.T.A Huysmans, Plasma Phys. Control. Fusion **47**, B165-B178 (2005)